

Visible continuous emission from a silica microphotonic device by third-harmonic generation

TAL CARMON AND KERRY J. VAHALA*

California Institute of Technology, 1200 E. California Boulevard, Pasadena, California 91125, USA

*e-mail: vahala@caltech.edu

Published online: 7 May 2007; doi:10.1038/nphys601

Nonlinear harmonic generation is widely used to extend the emission wavelength of laser sources. These devices typically require high peak powers to generate sufficient nonlinear optical response. Here, we demonstrate experimentally and analyse theoretically continuous-wave, visible emission from a silica microresonator on a silicon chip by third-harmonic generation. Emission is observed with pump powers of less than 300 μW , and is verified to scale cubically with pump power. We also observe third-order sum-frequency generation and mixing of the pump with a concomitant Raman laser within the same structure, giving rise to emission of various colours. In addition to providing low-power operation, this result opens the possibility of silicon microphotonic emitters spanning all the way down to the ultraviolet and operating continuously.

Silica glass has laid the foundation of the photonic revolution over the past decades as its durability and low optical loss over a broad spectral window has enabled light transmission over long distances by optical fibres. In this capacity, silica's role is both passive and active as erbium-based-fibre amplifiers^{1–3} are essential for signal regeneration. Moreover, silica is a mainstay of optical technology on-a-chip^{4,5}, including recent efforts to create new complementary metal-oxide-semiconductor (CMOS)-compatible optical device technologies (that is, silicon photonics). Furthermore, photonic-crystal fibre^{6,7} has paved the way for new phenomena and technologies useful for manipulation of light. In these new frontiers of silica-based applications, important underlying themes are to leverage a perfected technology (modern telecommunications in the 1.5 μm band and CMOS electronics) for potential new gains. In this paper, this idea is extended in a new way demonstrating a silica-on-silicon microplatform that links the telecommunications window to the visible spectrum.

Here, we demonstrate experimentally for the first time broadly tuneable, visible, continuous emission from a silica microphotonic device by third-harmonic (TH) generation. The micro-emitter is a CMOS-compatible silicon-photonics-based device, made of pure silica on a silicon chip. Third-harmonic emission in silica has been studied in the context of optical fibres⁸. However, the principle of operation in the current work extends previous work on nonlinear resonant enhancement in high-quality-factor optical microcavities. In particular, we build on the work of Chang who pioneered visible emission by using the TH nonlinearity in droplets^{9–11}. Our work also extends other liquid droplet work¹² as well as other nonlinear phenomena studied in liquids^{13,14} and solid spheres¹⁵ and later in toroidal resonators¹⁶. The visible TH is different to that of semiconductor sources¹⁷.

Third-harmonic light is observable at only 300 μW of pump power operating at room temperature. Phase matching is achieved by compensation of the material dispersion by the dispersion of the cavity modes. The ability to produce 500 nm light from a 1,500 nm

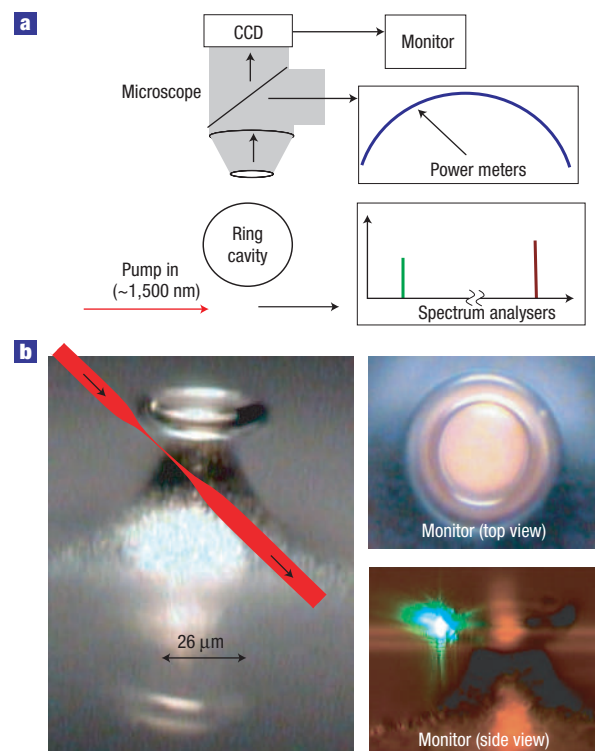


Figure 1 Experimental set-up. **a**, Infrared pump (of 300 kHz bandwidth) evanescently coupled to a microring cavity by a tapered fibre, generating visible TH emission. The TH emission is monitored by a camera, detector and a spectrum analyser. **b**, Left: The tapered fibre via which the pump is evanescently coupled into the ring cavity. Right: Top and side view of the cavity; TH power is visible in the side view.

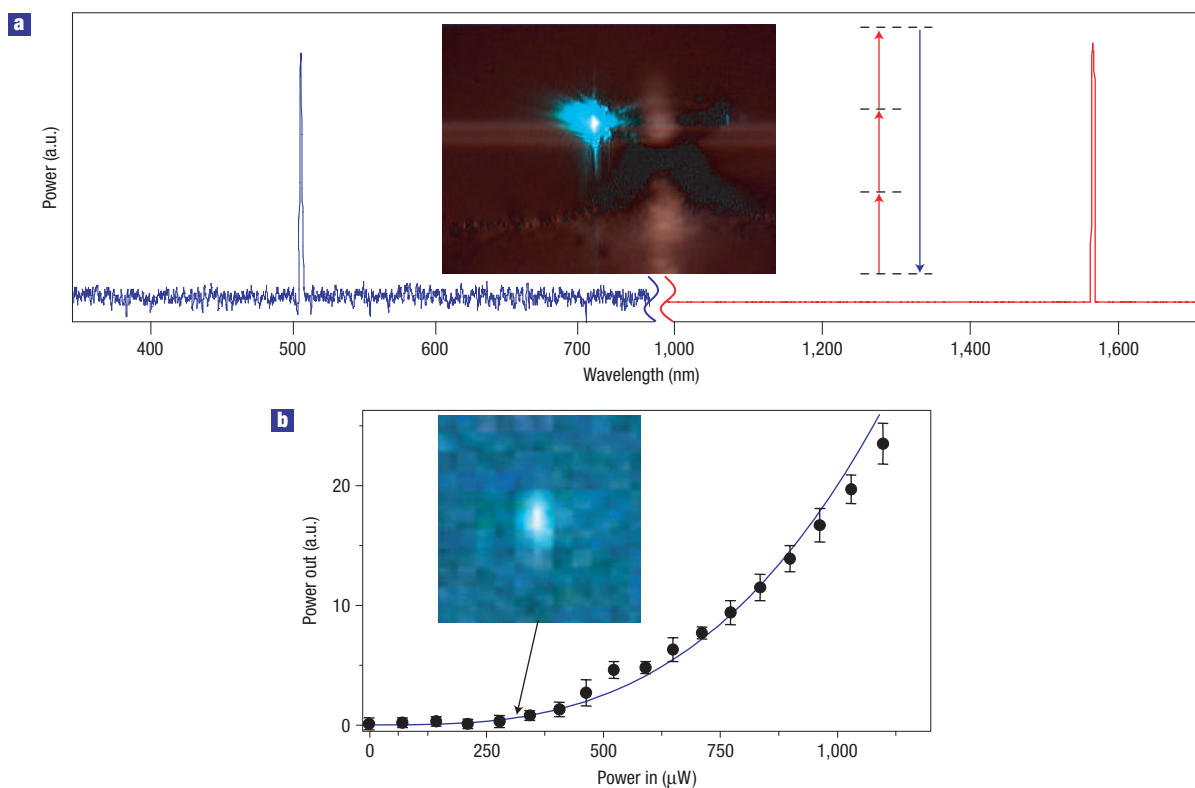


Figure 2 Experimental results. **a**, Measured spectrum showing the 517.4 nm TH (blue) of the 1,553.9 pump (red). The inset photograph was taken during the spectral measurement. The TH and the pump are not to the same scale. **b**, Measured TH power as a function of the pump input power. The solid curve is a cubic power fit to the data. The inset photograph taken at an input power of 300 μW demonstrates that even at this low power, TH is observable. The error bars provide the standard deviation over ~ 200 data points. The error in x is smaller than the point size. Toroid major and minor radii are 13 and 3.26 μm , and the quality factor was measured to be 2×10^7 at 1,500 nm.

pump, linking the mature capabilities of the near-infrared telecom sources directly to the centre of the visible band, is of particular interest. More generally, here the very broad silica window also enables the experimental demonstration of multicolour emission from the same device, allowing arbitrary-colour emission from a single platform. The potential capability to produce ultraviolet radiation is also significant.

Silica can function as a short-wavelength source as generation of the TH signal allows emission at three times the pump frequency, thereby conveniently linking the telecom band to the visible spectrum. Generally, third-order effects are masked by the much stronger¹⁸ second-order effects^{19–23}. An exception is centrosymmetric materials such as amorphous silica in which inversion symmetry forbids competing second-order processes and sets the TH process to be the first in line.

The TH power scales as pump-intensity cubed, and in resonant cavities, this cubic relation translates to converted power being proportional to $(Q/V)^3$, where Q is the cavity quality factor (inversely proportional to optical loss) and V is the volume of the optical mode. Therefore, reducing size and optical losses in a microresonator device will dramatically enhance the TH signal. Furthermore, as other competing phenomena generally scale as $(Q/V)^n$, where $n < 3$, the TH signal is not only absolutely intensified when Q/V is increased but is also enhanced in comparison with other optical phenomena.

The experiment takes advantage of resonance enhancement in an ultrahigh- Q microresonator made of silica²⁴ (Fig. 1). The

pump is coupled into the cavity via a fibre taper waveguide^{25,26}. To give a scale for the resonant enhancement achieved here, cavity Q and diameter are such that 1 mW of pump power launched on the optical fibre gives rise to 300 W circulating power in the cavity. This circulating power is concentrated to a typical modal cross-sectional area of only 2 μm^2 , thereby creating an intensity of approximately 10^{14} W m^{-2} . Measurements on the TH signal are done by collecting the TH light scattered from the cavity, or the TH light coupled via the taper (Fig. 1). The tapered coupler is designed for efficient coupling of the infrared pump. Although this coupler is not phase matched in the visible region, it does allow enough coupling of TH radiation to confirm physical aspects of the TH mechanism (for example, spectrum, pump power dependence). With the motivation of being able to efficiently couple both the infrared pump and the visible signal, we are now developing a wavelength-independent fibre coupler²⁷.

A typical measured emission spectrum is shown in Fig. 2a. In this case, pumping at 1,553.9 nm creates a TH signal occurring at 517.4 nm, deviating only 0.1% from the expected wavelength (1,553.9/3); deviation here is comparable to the spectrum analysers' resolution limit of 0.4 nm. No other emission lines were observed within the spectrum analysers' range (190–1,700 nm), demonstrating experimentally that TH emission is possible with no competition from other processes. The other processes are Raman and parametric oscillation^{15,16}, which exhibit a clear threshold pump power. Hence, by adjusting the threshold for either process, TH emission can occur unfettered. The suppression of parametric

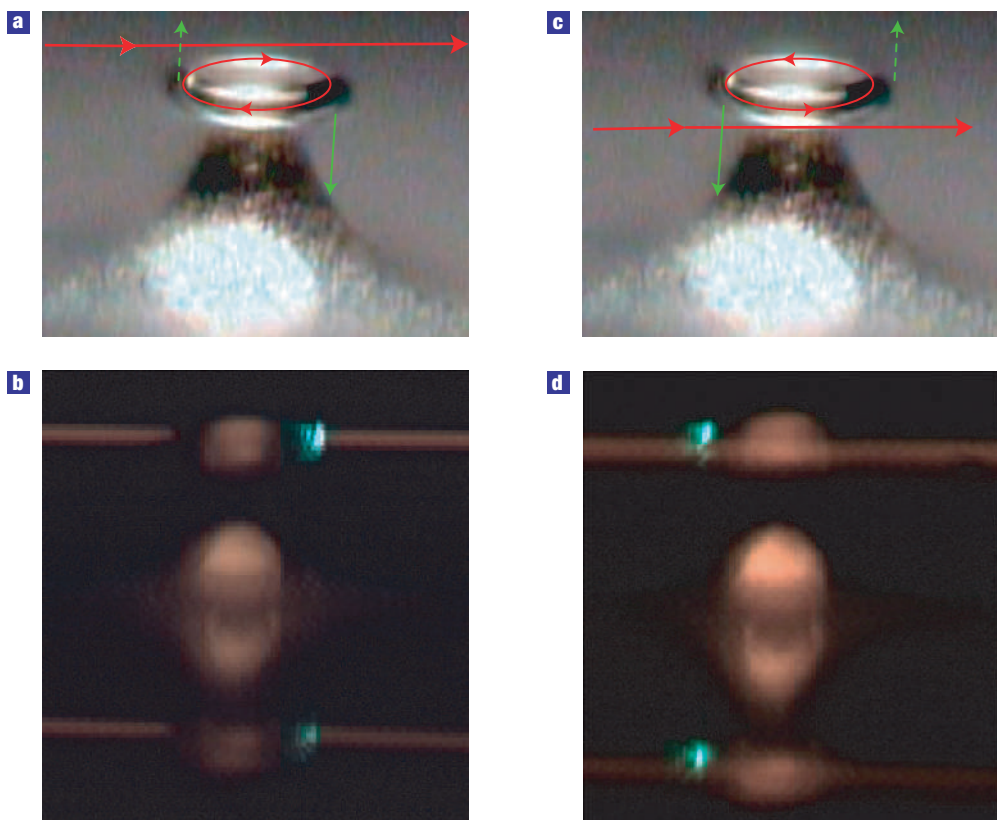


Figure 3 Observation of directional emission of the TH signal. Although the visible scattering is uniform around the ring, scattering is mainly forward and hence collected by the camera from a limited region. **a,b**, When the tapered fibre is coupled from behind the cavity (**a**), the pump circulates in the clockwise direction. In this case, the TH signal also has a clockwise circulation (**b**). Note that the double image results from the mirror image (in both **b** and **d**) of the resonator reflecting from the surface of the silicon wafer. **c,d**, When the pump is switched to rotate anticlockwise (by simply moving the tapered fibre to the other side of the cavity (**c**)), then the signal scattering is switched to the left-hand cavity side (**d**) indicating that the signal has switched its direction to co-circulate with the pump.

effects is well understood and involves adjustment of the toroidal aspect ratio as described in ref. 16. Furthermore, because Raman oscillation occurs in a distinct band of wavelengths in relation to the pump wave, controlling Raman emission by increasing its threshold (and without adverse effects on the TH process) is possible by introducing resonant absorption or resonant scattering in selected bands. The use of rare earths or the introduction of holographic index gratings, both of which have been successfully incorporated in either toroids²⁸ or silica microspheres²⁹, would provide two possible means to achieve this result. For example, the incorporation of erbium²⁸ would lower the Q (and hence raise the threshold) for Raman over a band near 1,500 nm. This would, in turn, free up operation from about 1,320 to 1,420 nm for TH pumping (with a corresponding emission from 450 to 473 nm). Gratings²⁹ could provide the opportunity to tune scattering (and thereby selectively Q spoil) of any desired band.

Measurement of the TH emission power as a function of pump power is shown in Fig. 2b. A logarithmic fit of the data gives an $x^{2.954}$ dependency of the TH signal on the pump power, deviating only 1.5% from the expected x^3 behaviour, and further confirming the TH nature of the process. From this cubic power dependency (and also from the measured spectra in Fig. 2a), we conclude that other effects, if they co-exist, were at least two orders of magnitude lower than the TH. The inset in Fig. 2b was taken at a pump power of less than 300 μW , demonstrating that even at low input power levels the TH signal is easily observable.

Another important feature of the TH emission is its direction. The basic principle of linear momentum conservation in the TH process imposes a requirement that clockwise circulating pump waves induce clockwise emission and vice versa (experimentally verified in Fig. 3). Confirmation of phase matching in a coarse, directional sense (as above) raises the question of precisely how phase matching occurs over such a broad wavelength range (that is, the near-infrared to visible range). Expressing the field in cylindrical coordinates as $E_i(r, z)e^{i(\omega_i t - \beta_i \phi)}$ ($E_i(r, z)$ is calculated numerically with a vectorial finite-difference mode solver assuming axial symmetry), momentum is conserved when the number of TH wavelengths along the circumference is three times that of the pump ($\beta_{\text{TH}} = 3\beta_p$). Although it is easy to find such a pair that satisfies momentum conservation, energy conservation ($\omega_{\text{TH}} = 3\omega_p$) is not *a priori* satisfied as dispersion generally causes the pump to circulate faster than the TH signal. More precisely, the generated TH power for the selected pair $\beta_{\text{TH}} = 3\beta_p$ is:

$$P_{\text{TH}} = \left(\frac{\chi^{(3)} \eta_0}{2\epsilon_0 n^2} \right)^2 \left(\frac{P_p Q_p \lambda_p}{2\pi r n A_p} \right)^3 \left(\frac{2\pi r n Q_{\text{TH}}}{A_{\text{TH}} \lambda_{\text{TH}}} \right)^4 \frac{\left| \int_{r,z} E_p^3 E_{\text{TH}}^* dA \right|^2}{4(\Delta\omega\tau_{\text{TH}})^2 + 1},$$

$$E_i = E_i(r, z), \quad A_i = \int_{r,z} |E_i|^2 dA, \quad \max |E_i|^2 = 1. \quad (1)$$

Here coupled-mode theory (for review, see ref. 30) is used for the case of a cavity with third-order nonlinearity and optical losses.

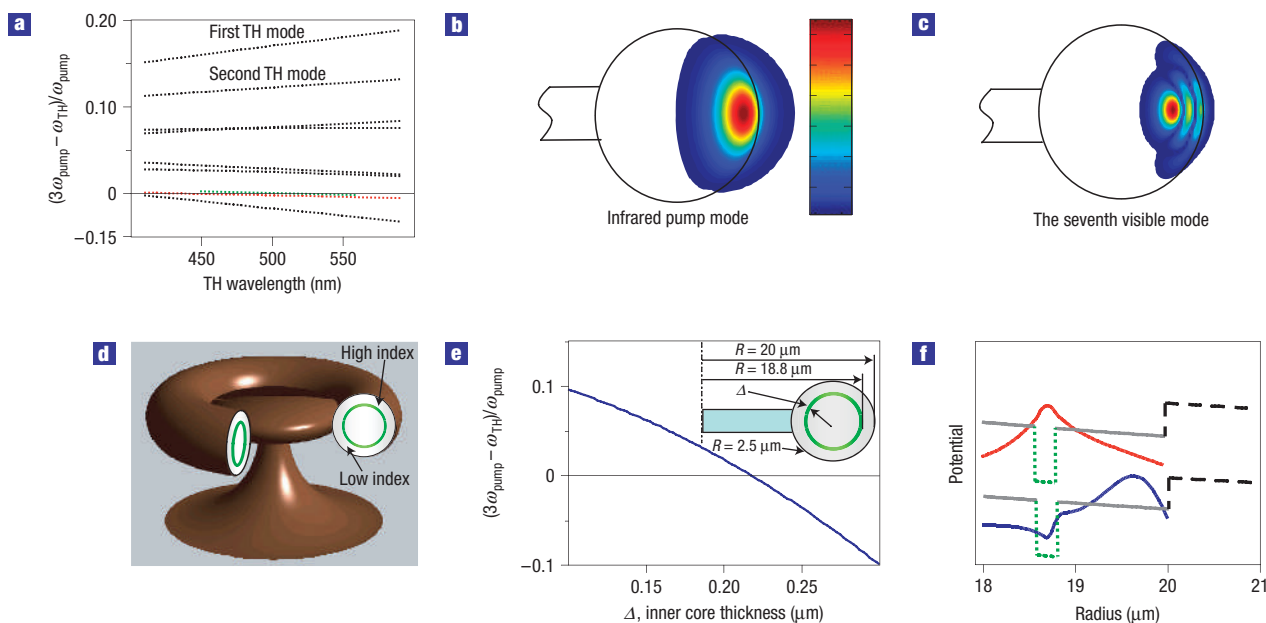


Figure 4 Phase matching between the infrared pump and the visible TH. **a**, Calculated normalized frequency mismatch between the pump mode and various TH modes versus TH wavelength. The intersection of the red line with the abscissa represents phase matching of the seventh visible TH mode with the pump fundamental infrared mode. The modes are numerically calculated for the cavity that was experimentally tested in Fig. 2b, where only symmetrical transverse-magnetic modes were considered. All pump–TH pairs satisfy momentum conservation ($\beta_{\text{TH}} = 3\beta_p$), and at the intersection with the abscissa, propagation constants were $\beta_{\text{TH}} = 270$ and $\beta_p = 90$. The green line illustrates the effect of increasing the cavity size by 10% on the phase-matching condition. The lines consist of a discrete set of resonances separated by a free spectral range of ~ 1 nm (to represent this fact, the lines are dotted). **b**, Electric-field distribution for the pump fundamental infrared mode. The colour bar indicates the relative intensities. **c**, Electric-field distribution for the seventh visible TH mode. **d–f**, A proposal for a future experiment. **d**, Adding a high-index layer (green) will allow phase matching between the fundamental TH and pump modes. **e**, Plot of normalized frequency mismatch between the fundamental pump and the TH mode as a function of the thickness of the high-index layer. The intersection with ‘zero’ represents phase matching. **f**, Calculated radial field distribution of the pump (red, top) and the TH (blue, bottom) drawn over the approximate effective potential where the grey (solid), green (dotted) and black (dashed) lines represent silica, Si^3N^4 and air.

n is the refractive index, $\chi^{(3)}$ is the third-order susceptibility, ε_0 is the vacuum permittivity, λ is the optical wavelength and $\eta_0 = 377 \Omega$. P and Q are the coupled power and quality factor. A is the mode area calculated by integrating the normalized field over the plane transverse to the propagation direction (the r, z plane). The scaling $Q_p/(2\pi r)$ reflects the power build-up factor (that is, circulating power/input power), whereas the $1/A_p$ dependence reflects the fact that it is intensity that counts in the TH process. The cubic dependence of the TH power on circulating pump intensity is evident from the second term. The numerator of the last term is the spatial overlap integral between the electric field of the pump and the TH field. The last-term denominator, which accounts for the effect of dispersion-induced phase mismatch (as given by $\Delta\omega = 3\omega_p - \omega_{\text{TH}}$) in the resonant system, is of special interest. In particular, the phase difference between the pump and the TH ($\Delta\omega\tau_{\text{TH}}$) acquired during the TH photon lifetime (τ_{TH}) should be small for proper phase matching. An important degree of freedom, in this regard, is the existence of high-order transverse modes for the TH signal. In Fig. 4a, we calculate $\Delta\omega$ for various TH transverse modes that satisfy $\beta_{\text{TH}} = 3\beta_p$. When the TH mode order is high enough, TH mode dispersion via extension into the air cladding can fully compensate material and waveguide dispersion. Furthermore, Fig. 4a also shows that the wavelength of the optimal matching can be controlled through adjustment of the cavity dimensions. Such mode-match techniques have been used in optical fibres^{8,31}; furthermore, the fact that clad–core index contrast here ($\Delta n = 0.46$) is much higher than in fibres is important in helping to compensate dispersion by using

high-order TH modes. As expected, we experimentally observe in Fig. 5a (with a high-numerical-aperture lens) that all of the TH modes exhibited internal nodes (that is, non-fundamental mode), although the precise number of nodes was not easily resolved.

This method of phase matching has several disadvantages. In particular, the complex structure of the TH mode reduces its spatial overlap with the pump and also with the fibre taper used to couple to the toroid. Furthermore, the high-order TH mode of the toroid does not phase match well to the fibre taper when the fibre taper is, itself, first phase matched to the infrared pump wave. The combination of these factors weighs heavily on the fibre–taper coupling efficiency of the TH wave. In particular, whereas the pump wave enjoys an excellent efficiency (in excess of 90% from the fibre input), the TH coupling efficiency is in the range of 1%. In this regard, excitation of an appropriately phase-matched, TH, fundamental transverse mode would be highly preferable. An alternative structure shown in Fig. 4d can provide a means to address this issue. In this toroidal resonator, a sandwiched layer of high-index Si^3N^4 core is (chemical-vapour) deposited between a toroidal silica core and an outer layer of silica, as shown in the figure. In Fig. 4e, we calculate $\Delta\omega/\omega_p$ (for a mode pair with $\beta_{\text{TH}} = 3\beta_p$) as a function of the nitride layer width. The intersection with the abscissa gives the width required for phase matching; and the calculated field distribution in Fig. 4f possesses overlap between TH and pump modes that is much better than for the mode-match method (from Fig. 4a). The TH mode ‘fundamental’ transverse profile also overlaps well with the fibre taper structure. Here, a quantum-mechanical analogy³², provided by plotting the ‘effective’

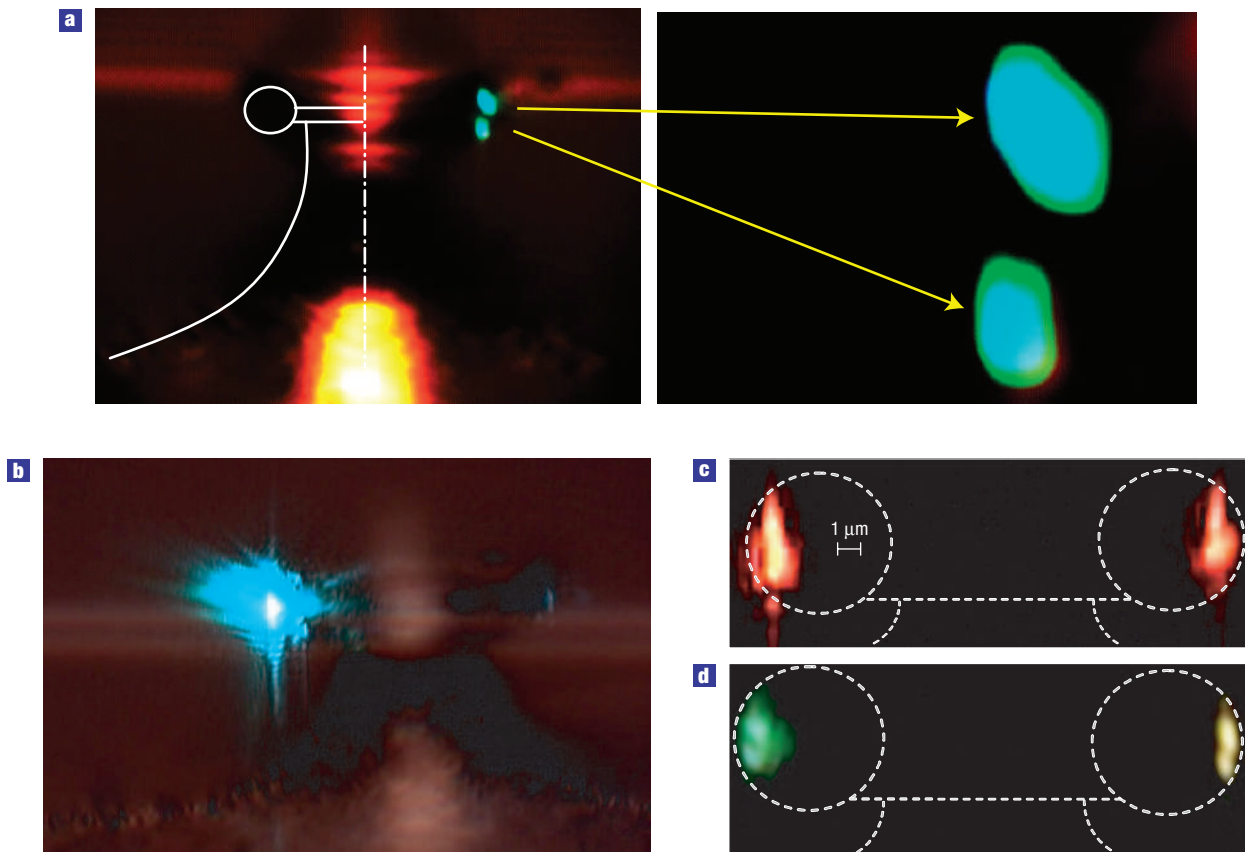


Figure 5 Experimental observation of internal modes and multicolour generation. **a**, Use of a high-numerical-aperture objective allows imaging internal node structure in the TH mode. We note that the fine mode structures are difficult to image. The white lines represent the approximate geometry of the toroid cross-section. **b**, A unidirectional signal is generated by a unidirectional pump. **c**, Two, identical, counter-rotating pumps give rise to two counter-rotating signals. **d**, Two different pumps that also counter rotate are giving rise to two counter-rotating signals of different colour.

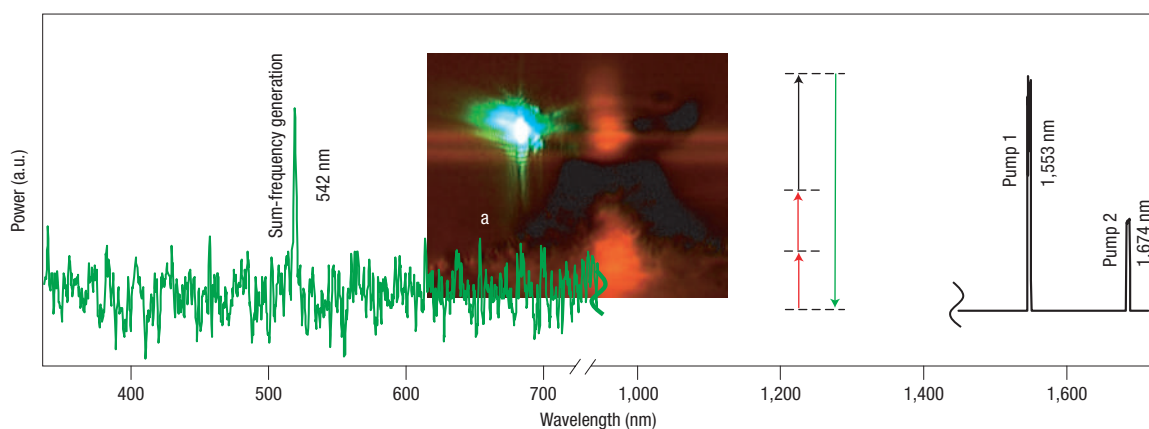


Figure 6 Measured spectra showing third-order sum-frequency generation where two 1,674 nm photons are summed with one 1,553 nm photon to generate emission at 542 nm. The inset photograph was taken during the spectral measurement; the signal and pump are not to the same scale.

optical potential (along the radial direction) perceived by the modes in the silica/nitride microcavity, is useful in understanding the function of the nitride layer. Using the wave equation in

spherical coordinates to approximate the situation, Fig. 4f reveals a double-welled potential in which the TH wave populates the outer well, whereas the pump wave populates the (high-index silicon

nitride) inner well (and hence is selectively slowed down). Using equation (1), the efficiency for this Si^3N^4 core device (Fig. 4d) can be as high as 53% for a $140\ \mu\text{W}$ pump (Q_p is the one measured in Fig. 2b; Q_{TH} is assumed to be equal to Q_p and the wavelength-dependent refractive indices for the Si^3N^4 and SiO_2 were taken from ref. 33). This efficiency is high enough that pump depletion (which has not been included in the analysis) would undoubtedly be a factor even at these relatively low input powers. Developing this multilayer technology is beyond the scope of this article and is a matter for future research.

The broad silica transmission window has the virtue of not limiting the device to a single colour output. This is shown experimentally in Fig. 5b–d where several colours are photographed from the same device. Simultaneous, two-colour emission is also shown in Fig. 5d. In a similar manner, more than two colours could be generated within the same device to synthesize arbitrary-colour emission originating from a single platform. Yet another degree of freedom here is the possibility to generate not only the TH signal but also the third-order sum frequency from two (or even three) different pump wavelengths: one such example measured here (Fig. 6) is the generation of emission at 544 nm by summation of two different frequencies from a pump and concomitant Raman signal ($2/1,674 + 1/1,553 = 1/544$).

To summarize, we demonstrated a durable device that exploits TH generation for continuous visible emission. In addition to the observation of continuous-wave TH emission, we did not observe any Q degradation or damage to the devices, even using pump intensities as high as 1 W (using an erbium-fibre amplifier to boost the power of the pump laser). Although the devices used here are currently unique in terms of providing ultrahigh Q in a wafer-compatible, microscale platform, the sustained trend in Q/V microcavity performance^{34–36} suggests that similar devices over a wide range of platform types will soon be possible. In particular, a non-reflow strategy to achieve Q factors of 50 million has recently been demonstrated³⁷. Such an approach simplifies process compatibility with CMOSs. Recent advances in high- Q photonic-crystal microresonators³⁸ are also intriguing, as such structures achieve very high Q/V and could potentially provide dispersion engineering techniques useful to address phase matching of the pump and TH signal. Therefore, we consider the present embodiment demonstrated here as being just one of many possibilities that will be enabled by continued progress within the broad field of microcavity research. Finally, a natural extension of this work will be the use of the broad silica transmission band to generate tuneable, ultraviolet emission using the present device. Because of the cubic pump-band Q -factor dependence, efficient emission into the deep-ultraviolet band (for example, 780 nm sources to 260 nm TH) should be possible using this silica-based structure. Furthermore, the emitting platform is not limited to be made of silica and, in principle, any transparent centrosymmetric material can be used; among these materials, CaF_2 is of particular interest as high- Q cavities made of this material (CaF_2) were already demonstrated experimentally³⁹ and it possesses capabilities for extreme-ultraviolet emission as its transparency window goes down to 160 nm. In the future, replacing the 1,550 nm source with a 780 nm input to obtain ultraviolet TH will also allow shrinking of the cavity by the same ratio without suffering increased radiation loss. As TH scales with $(Q\lambda/V)^3$, this size reduction means a higher efficiency conversion (assuming similar Q) when compared with the current visible result. Even though current Q factors are not limited by silica's intrinsic loss, this component of Q will probably be higher in the ultraviolet region. Hence, the same size scaling effect can help to extend efficient operation into the ultraviolet region.

Received 11 December 2006; accepted 29 March 2007; published 7 May 2007.

References

- Desurvire, E. *Erbium-Doped Fiber Amplifiers: Principles and Applications* (Wiley, New York, 1994).
- Becker, P. C., Olsson, N. A. & Simpson, J. R. *Erbium-Doped Fiber Amplifiers: Fundamentals and Technology* (Academic, San Diego, 1999).
- Digonnet, M. J. F. *Rare-Earth-Doped Fiber Lasers and Amplifiers* 2nd edn (Dekker, New York, 2001).
- Boyrav, O. & Jalali, B. Demonstration of a silicon Raman laser. *Opt. Express* **12**, 5269–5273 (2004).
- Liu, A. S. *et al.* A high-speed silicon optical modulator based on a metal–oxide–semiconductor capacitor. *Nature* **427**, 615–618 (2004).
- Knight, J. C. Photonic crystal fibres. *Nature* **424**, 847–851 (2003).
- Knight, J. C., Birks, T. A., Russell, P. S. & Atkin, D. M. All-silica single-mode optical fiber with photonic crystal cladding. *Opt. Lett.* **21**, 1547–1549 (1996).
- Bufetov, I. A., Grekov, M. V., Golant, K. M., Dianov, E. M. & Khrapko, R. R. Ultraviolet-light generation in nitrogen-doped silica fiber. *Opt. Lett.* **22**, 1394–1396 (1997).
- Acker, W. P., Leach, D. H. & Chang, R. K. Third-order optical sum-frequency generation in micrometer-sized liquid droplets. *Opt. Lett.* **14**, 402–404 (1989).
- Leach, D. H., Acker, W. P. & Chang, R. K. Effect of the phase-velocity and spatial overlap of spherical resonances on sum-frequency generation in droplets. *Opt. Lett.* **15**, 894–896 (1990).
- Leach, D. H., Chang, R. K., Acker, W. P. & Hill, S. C. Third-order sum-frequency generation in droplets—experimental results. *J. Opt. Soc. Am. B* **10**, 34–45 (1993).
- Kasparian, J. *et al.* Angular dependences of third harmonic generation from microdroplets. *Phys. Rev. Lett.* **78**, 2952–2955 (1997).
- Qian, S. X. & Chang, R. K. Multiorder Stokes emission from micrometer-size droplets. *Phys. Rev. Lett.* **56**, 926–929 (1986).
- Lin, H. B., Eversole, J. D. & Campillo, A. J. Continuous-wave stimulated Raman-scattering in microdroplets. *Opt. Lett.* **17**, 828–830 (1992).
- Spillane, S. M., Kippenberg, T. J. & Vahala, K. J. Ultralow-threshold Raman laser using a spherical dielectric microcavity. *Nature* **415**, 621–623 (2002).
- Kippenberg, T. J., Spillane, S. M. & Vahala, K. J. Kerr-nonlinear optical parametric oscillation in an ultrahigh-Q toroid microcavity. *Phys. Rev. Lett.* **93**, 083904 (2004).
- Ponce, F. A. & Bour, D. P. Nitride-based semiconductors for blue and green light-emitting devices. *Nature* **386**, 351–359 (1997).
- Boyd, R. W. *Nonlinear Optics* 2nd edn (Academic, San Diego, 2003).
- Franken, P. A., Weinreich, G., Peters, C. W. & Hill, A. E. Generation of optical harmonics. *Phys. Rev. Lett.* **7**, 118–120 (1961).
- Osterberg, U. & Margulis, W. Dye-laser pumped by Nd-YAG laser-pulses frequency doubled in a glass optical fiber. *Opt. Lett.* **11**, 516–518 (1986).
- Myers, R. A., Mukherjee, N. & Brueck, S. R. J. Large second-order nonlinearity in poled fused-silica. *Opt. Lett.* **16**, 1732–1734 (1991).
- Dominic, V. & Feinberg, J. Light-induced second-harmonic generation in glass via multiphoton ionization. *Phys. Rev. Lett.* **71**, 3446–3449 (1993).
- Ilchenko, V. S., Savchenkov, A. A., Matsko, A. B. & Maleki, L. Nonlinear optics and crystalline whispering gallery mode cavities. *Phys. Rev. Lett.* **92**, 043903 (2004).
- Armani, D. K., Kippenberg, T. J., Spillane, S. M. & Vahala, K. J. Ultra-high-Q toroid microcavity on a chip. *Nature* **421**, 925–928 (2003).
- Knight, J. C., Cheung, G., Jacques, F. & Birks, T. A. Phase-matched excitation of whispering-gallery-mode resonances by a fiber taper. *Opt. Lett.* **22**, 1129–1131 (1997).
- Cai, M., Painter, O. & Vahala, K. J. Observation of critical coupling in a fiber taper to a silica-microsphere whispering-gallery mode system. *Phys. Rev. Lett.* **85**, 74–77 (2000).
- Wang, S., Carmon, T., Ostby, E. P. & Vahala, K. J. *Quantum Electronics and Laser Science Conference, May 7, Baltimore, USA* (accepted for oral presentation, 2007).
- Yang, L., Armani, D. K. & Vahala, K. J. Fiber-coupled erbium microlasers on a chip. *Appl. Phys. Lett.* **83**, 825–826 (2003).
- Ilchenko, V. S., Starodubov, D. S., Gorodetsky, M. L., Maleki, L. & Feinberg, J. *Conference on Lasers and ElectroOptics 67* (Optical Society of America, Baltimore, 1999).
- Haus, H. A. & Huang, W. P. Coupled-mode theory. *Proc. IEEE* **79**, 1505–1518 (1991).
- Stolen, R. H., Bjorkhol, J. & Ashkin, A. Phase-matched 3-wave mixing in silica fiber optical-waveguides. *Appl. Phys. Lett.* **24**, 308–310 (1974).
- Johnson, B. R. Theory of morphology-dependent resonances—shape resonances and width formulas. *J. Opt. Soc. Am. A* **10**, 343–352 (1993).
- Baak, T. Silicon oxynitride—a material for grin optics. *Appl. Opt.* **21**, 1069–1072 (1982).
- Savchenkov, A. A., Ilchenko, V. S., Matsko, A. B. & Maleki, L. Kilohertz optical resonances in dielectric crystal cavities. *Phys. Rev. A* **70**, 051804 (2004).
- Robinson, J. T., Manolatou, C., Chen, L. & Lipson, M. Ultrasmall mode volumes in dielectric optical microcavities. *Phys. Rev. Lett.* **95**, 143901 (2005).
- Vahala, K. J. Optical microcavities. *Nature* **424**, 839–846 (2003).
- Kippenberg, T. J., Kalkman, J., Polman, A. & Vahala, K. J. Demonstration of an erbium-doped microdisk laser on a silicon chip. *Phys. Rev. A* **74**, 051802 (2006).
- Akahane, Y., Asano, T., Song, B. S. & Noda, S. High-Q photonic nanocavity in a two-dimensional photonic crystal. *Nature* **425**, 944–947 (2003).
- Savchenkov, A. A. *et al.* Low threshold optical oscillations in a whispering gallery mode CaF_2 resonator. *Phys. Rev. Lett.* **93**, 243905 (2004).

Acknowledgements

We acknowledge helpful discussions with M. Shumate, J. Scheuer and A. Yariv and support from the Caltech Lee Center and DARPA. T.C. acknowledges a fellowship from the Center for the Physics of Information at Caltech. Correspondence and requests for materials should be addressed to K.J.V.

Author contributions

T.C. fabricated the devices, carried out the experiments, analysed the data and derived the analytical and numerical calculations. K.J.V. supervised all aspects of this project. Both authors made contributions to the concepts demonstrated and proposed in the article.

Competing financial interests

The authors declare no competing financial interests.

Reprints and permission information is available online at <http://npg.nature.com/reprintsandpermissions/>